A R C H I V E S O F M E T A L L U R G Y A N D M A T E R I A L S
Volume 53 2008 Issue 3

M. SUŁOWSKI*, P. DUDEK*

THE EFFECT OF COOLING RATE ON THE STRUCTURE, POROSITY AND MECHANICAL PROPERTIES OF SINTER-HARDENED Fe-3%Mn-0.8%C PM STEELS

WPŁYW SZYBKOŚCI CHŁODZENIA NA STRUKTURĘ, POROWATOŚCI I WŁASNOŚCI MECHANICZNE SOIEKANYCH STALI MANGANOWYCH Fe-3%Mn-0,8%C PM STEELS

New applications for manganese PM steels are continuously introduced on the market. Many of these new applications utilize the unique possibilities of powder metallurgy to achieve high strength in combination with close dimensional tolerances and to minimize the manufacturing operations. The mechanical properties of PM steels are affected by many factors, including the green and as-sintered densities, porosity, sintering temperature, sintering atmosphere and cooling rate.

In this paper the influence of cooling rate on structure, porosity and mechanical properties of sintered manganese PM steels is discussed. The materials used was Fe-3%Mn-0.8%C steel, prepared of commercial iron powder, finely ground Fe-77%Mn-1.3%C low-carbon ferroalloy, and carbon added in the form of graphite powder. Following mixing in double cone laboratory mixer, the mixtures of powders were cold compacted into standard tensile specimens according to ISO 2740/MP1F or rectangular specimens, 55×10×5 mm in size. Zinc stearate was used for die wall lubrication. To achieve green densities ~7.0 gcm^{-3}, the pressing pressure was 660 MPa for "dogbone" specimens and 820 MPa for rectangular specimens. Sintering was carried out in laboratory furnace at 1120°C and 1250°C. After sintering, the specimens were cooled to the room temperature at different cooling rates (4.5-65°C/min). The hydrogen atmosphere with -60°C dew point was used to prevent of sublimation and oxidation of the manganese. Densities (green and as-sintered) of samples varied from 6.87 gcm^{-3} to 7.02 gcm^{-3} for "dogbone" and from 6.91 gcm^{-3} to 7.03 gcm^{-3} for rectangular specimens. The porosity analysis and microstructure investigations were pursued using light-optical microscope. The measured values of mean equivalent circular diameter (ECD) and mean pore area for specimens sintered at 1250°C were consistently lower, than for their counterparts sintered at 1120°C. However higher internal porosity was observed in samples sintered at 1250°C. The sintered microstructures were sensitive to the cooling rate. Slow furnace cooling between 4-9°C/min resulted in pearlitic structures for sintering temperature 1120°C and pearlitic structures with some ferrite for specimens sintered at 1250°C. Martensite, fine pearlite, bainite and retained austenite characterize the steel cooled from 40°C/min to 65°C/min rate.

Keywords: powder metallurgy (PM), PM manganese steels, porosity characterisation, mechanical properties

Stale manganowe, produkowane metodami metalurgii proszków, znajdują coraz szersze zastosowanie, z których wiele wskazuje na możliwość otrzymania wyrobów spiekanych o wysokich własnościach wytrzymałościowych w połączeniu z małymi tolerancjami wymiarowymi przy niskich nakładach kosztów. Własności mechaniczne spiekanych stali zależą od wielu czynników takich jak gęstość, temperatura i atmosfera spiekania oraz prędkość chłodzenia.

W pracy opisano wpływ prędkości chłodzenia na strukturę, porowatość i własności mechaniczne spiekanych stali manganowych. Badanym materiałem była stal o składzie Fe-3%Mn-0,8%C, wykonana z proszku żelaza NC100.24, proszku niskowęglowego żelazomanganu (Fe-77%Mn-1.3%C) oraz proszku grafitu C-UF. Mieszanie realizowano w mieszalniku dwustożkowym. Z przygotowanej mieszanki proszków, metodą jednokrotnego prasowania w stalowej matrycy, wykonano dwa rodzaje wyprasek: zgodne z PN-EN ISO 2740, przeznaczone do badań wytrzymałości na rozciąganie oraz prostopadłościenne, o wymiarach 55×10×5 mm, przeznaczone do badań wytrzymałości na zginanie, udarności oraz twardości. W procesie prasowania próbek, jako środek poślizgowy zastosowano stearynian cynku w celu zabezpieczenia stempli i ścianek matryc przed uszkodzeniem. Wypraski spiekano w wodorze o punkcie rosy -60°C w dwóch temperaturach: 1120°C i 1250°C. Po spiekaniu kształtki chłodzono prędkościami zmieniającymi się w zakresie od 4,5°C do 65°C. Zastosowanie podczas spiekania próbek wodoru miało na celu zapobieżenie sublimacji i tworzenia się tlenków manganu. Gęstości wyprasek i spieków wynosiły odpowiednio 6,87 g/cm^3 i 7,02 g/cm^3 dla próbek wytrzymałościowych oraz 6,91 g/cm^3 i 7,03 g/cm^3 dla próbek prostopadłościennych. Analiza porowatości została wykonana na podstawie obserwacji mikroskopowych spieków. Uzyskane wartości średniej średnicy zastępczej (ECD) i średniej powierzchni porów dla próbek spiekanych w temperaturze 1250°C były niższe niż dla próbek spiekanych

* FACULTY OF METALS ENGINEERING AND INDUSTRIAL, COMPUTER SCIENCE, AGH-UNIVERSITY OF SCIENCE AND TECHNOLOGY, 30-059 KRAKÓW, 30 MICKIEWICZA AV., POLAND

w temperaturze 1120°C. Stale spiekane w temperaturze 1250°C charakteryzowały się większą wewnętrzną porowatością. W wyniku chłodzenia próbek w zakresie prędkości od 4,5°C/min do 16°C/min uzyskano strukturę perlityczną z niewielką ilością ferrytu lub bainitu. W spiekach chłodzonych z prędkością 30°C/min występował bainit górny, drobny perlit oraz bainit dolny i martenzyt, odpowiednio dla temperatur spiekania 1120°C i 1250°C. Dalszy wzrost szybkości chłodzenia powodował tworzenie się w strukturze spieków bainitu igłastego, martenzytu i austenitu szczątkowego.

1. Introduction

Alloys for ferrous structural PM parts are essentially low to medium carbon low alloy steels containing varying amounts of either or both cooper and nickel, and often, small amount of more expensive molybdenum. This is because these elements have easily reducible oxides and their use has been dictated by production equipment and manufacturing constraints rather than by sound of metallurgical reasoning. Manganese would be an obvious choice for such high strength application if only this element could be protected from oxidation during sintering [1]. Cias and co-workers [2-5] overcame this problem in laboratory and pilot scale. It is now widely recognised that the mechanical properties and dimensional changes of the sintered manganese steels depend on grade of the iron powder and sintering temperature variations and also at different sintering atmosphere dew point level [6]. Manganese PM steels exhibit smaller dimensional scatter than those containing copper.

Present developments towards high performance PM ferrous structural parts include alloy modifications involving also chromium and manganese, as evidenced by Höganäs Astaloy CrM powder with 3 wt.-% Cr [7] and Mn contents in some of Stackpole's alloys approaching 1% [6, 8, 9]. In different laboratories alloys containing up to 4 wt. -% Mn and 3 wt. -% Cr have been reproducibly PM processed without the formation of the deleterious oxide networks [1-4, 10-15]. Although tensile strengths can approach 1000 MPa with 2% ductility [4, 14], the alloy compositions and heat treatments remain to be optimised.

The reaction of manganese with various sintering atmospheres was the subject of works [15, 16]. Oxidation of manganese can be overcome by using iron powders with low contents of oxygen, and ferromanganese powders. The cold single-pressed and sintered PM steels, with correctly chosen composition, made from different grades of iron and ferromanganese powders, sintered at 1250°C or at lower temperatures in combination with use of atmosphere with very low dew point and oxygen content, can reach tensile strength values above 700 MPa [16]. It is possible to attain strengths in excess of 1 GPa in such PM manganese steel [18, 19]. These high strength values are achieved only at certain contents of combined carbon in the alloy. In order to avoid decarburization and oxidation during sintering in wet hydrogen or hydrogen/nitrogen atmosphere, the Fe-Mn-C alloy must be protected from decarburization and oxidation by using semi-closed containers or gettered boxes [1].

The strength of a sintered alloy steel component is limited by the largest flaw size present. These flaws arise from pores and oxides present in the initial powder and green compact. Hence, in order to manufacture stronger PM steel, the starting powder must be processed in a manner that either reduces the size of the Mn oxide aggregates or eliminates them entirely. That can be achieved by low dew point local microatmosphere processing of the green compact [20]. The Fe-3%Mn-0.8%C alloy has been developed over a four-year research programme [1], in which major effort has concentrated in controlling oxygen pickup during sintering. This problem arises because of the high oxygen affinity of manganese. Brittleness in manganese steels processed in „wet" atmospheres is associated with the formation of continuous oxide networks; eliminating their formation by sintering in an atmosphere adhering to the Ellingham-Richardson oxide reduction criteria is responsible for a transition to ductility [16, 20, 24].

The vapour pressure of manganese has decisive effect on sintering alloying Mn steel. It is evident that in Fe-3%Mn alloy sintered at 1120°C the Mn vapour volume, generated by manganese sublimation in the compact is considerably higher than the pore volume [25-28]. Sublimation of manganese leads to capillary penetration of Mn vapour and formation of large secondary pores at the sites of sublimed particles of the alloying added ferromanganese powder [20].

In this study, green compacts were prepared and their sintering behaviour as well as the importance of their porosity for diffusion-induced changes in microstructure was investigated. These preliminary tests aimed on achieving information on the internal porosity as well as the amount and size of the micro-scale defects inside the consolidated and sintered Mn steel object. The purpose of this study was also to determine the effects of different techniques of PM steel preparation on porosity in a sintered compact.

2. Materials and methods

Commercial sponge iron powder was used to prepare the Fe-3%Mn-0.8%C PM alloy. Manganese was introduced as finely ground Fe-77%Mn-1.3%C low-carbon

ferroalloy with particle size below 40 μm and median of 15 μm (Table 1 and Fig. 1); carbon was introduced as C-UF graphite (Fig. 2). Mixing was performed with a double-cone mixer at 60 rpm for a period of 60 minutes.

TABLE 1
Chemical composition of ferromanganese powder after screening to <40μm

Ferromanganese type	Chemical composition of the ferromanganese powders, wt.-%				
	Mn	C	O	N	Fe
Elken II	76.96	1.3	0.19	0.02	Bal.

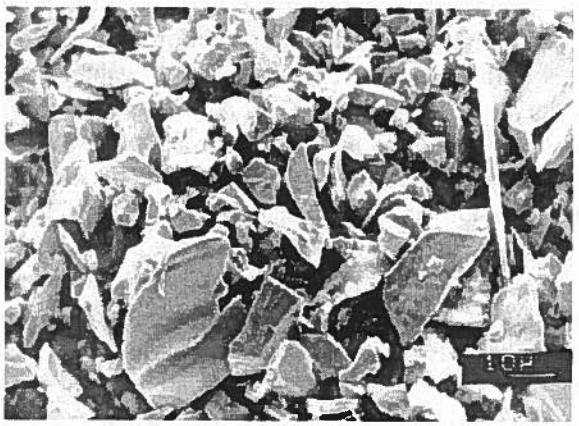

Fig. 1. SEM micrograph and particle size distribution of Elkem ferromanganese powder

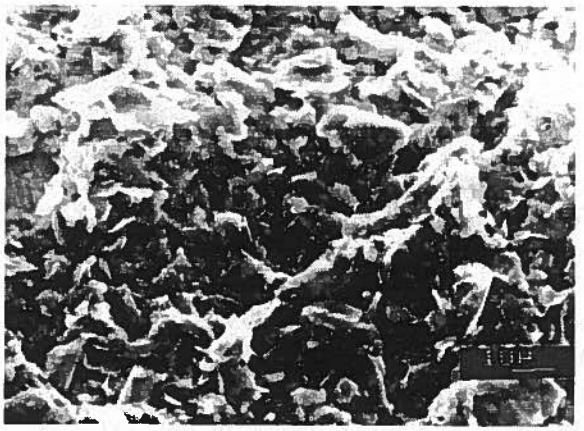

Fig. 2. SEM micrograph of graphite powder

Zinc stearate was used for die wall lubrication and the powders were compacted into standard "dogbone" tensile specimens conforming to ISO 2740/MPIF Standard 10 or rectangular specimens, 55×10×5 mm. The pressing pressures were 660 and 820 MPa, respectively, to achieve green densities in the range of ~7.0 gcm^{-3}. The lower punch was stationary during compaction. Compacts dimensions were measured with an electronic micrometer and the specimens were weighed on an analytical balance.

Sintering was carried out for 1 hour in a pure hydrogen atmosphere with -60°C dew point, in a laboratory furnace having Kanthal APM tube, at 1120°C or 1250°C.

In order to reduce manganese sublimation and oxidation, the specimens were placed in semi-closed container and slowly moved into the sintering zone. At the end of the sintering operation the specimens were moved to the water-cooled end of the tube for "convective" cooling. The ranges of cooling rates (CR), determined between 800°C and 300°C, summarised in Tables 3 and 5, were investigated. Chemical analyses of sintered Mn steels showed, in addition to minor manganese loss, some (0.2-0.3 %) decarburization of the steels with concurrent oxygen losses of up to 0.2%. So, although the steels nominally contained 0.8 wt.-% of carbon, the actual carbon contents of specimens sintered at 1120 and 1250°C were ~0.6 and ~0.5 wt. -% of carbon, respectively.

The results of two separate techniques were checked against each other and then used to evaluate various strength parameters of the steel: the tensile strength (TS) and transverse rupture strengths (TRS). TRS and TS of the specimens were measured with MTS testing machine. Beams like rectangular cross section specimens were prepared from the consolidated powder and tested in 3-point bending. The TRS were calculated according to Navier formula.

The percent porosity was calculated in support about Archimedes law. The specimens were observed and analysed using an optical microscope. This system uses a standard light microscope, digital camera, capture card to give the operator live video of the sample on the polished section and software for accurate particle distribution information. Resolution limits most reproducible analysis by optical microscopy to approximately 1 μm pores with theoretical resolution limit of about 0.2 μm (depend upon wavelength of illumination source). Eleven polished section images of the specimens were obtained vertically along the height of the specimens (Fig. 4.). The images were digitally reconstructed and the sizes, numbers and total volume ratio of the pores, which existed in the specimens, were determined. Digitalisation was the process of converting the continuously varying voltage output of the video signal into a discrete array of pixels whose values corresponded to the intensity of the parts of the original image that they represented. The percentage of porosity exposed by this was then measured by digital imaging the sample, designating (via

SigmaScan Pro 4.0 computer program) what areas were "void" (porous) areas, and dividing that area by the total area of the sample. This technique complies with ASTM Standard E1245-00, which addresses porosity measurement [29]. The modular structure of the software used allows the self-creation of needed algorithms for porosity characterisation and surface flaw detection. A big library of graphical tools for camera and light control, classical images treatment, comprehensive list of image types ensures image compatibility- including up to 16-bit gray scale images, porosity data inversion, mathematical tools, visualisation and data stocking permit an easy creation of special image analysis routines.

To investigate the porosity of sintered PM manganese steel the following parameters were measured:

- *The area of the pore (S)*, calculated directly from the pore pixel count on the camera sensor.
- *Area fraction* – the area of the pores represented as the proportion of the image that the pores occupy.
- *Perimeter (P)* – the length of the pore perimeter calculated from the pore pixel count on the camera sensor.

Pores sizes were expressed using calculated parameter, equivalent circular diameter (ECD), used mostly for optical microscopy-based technique where the profile of the three-dimensional pore is observed on two-dimensional plane. ECD is the diameter of a circle having the same area as the image of the pore, also known as Haywood Diameter [26]. If the area of a measured pore is S the equivalent circular diameter is calculated as

$$ECD = \sqrt{\frac{4 \cdot S}{\pi}} \quad (1)$$

Pore size and size distribution data can be presented in varied forms. Recognising that there is no single definition of pore size, ISO 9276-1: 1998 standard defines particle size as the diameter of a sphere having the same volume; this is known as equivalent spherical diameter. This standard concentrates on issues pertaining to the graphical representation of particle size analysis data, particularly as represented in the forms of histograms, density distributions and cumulative distributions. The distributions in questions apply not only to powders, but also to pores, over any size range.

3. Porosity characterisation by microscopy-based technique

Optical microscopy was performed on the samples in order to correlate the results obtained from the Archimedes' principle to the metallographically measured. Samples were examined for internal porosity content by mounting them in "metallographic" mounts, grinding them down and polishing.

In porous materials gas phase appears in the form of a Y^3 (three-dimensional) set of convex bodies (pores) distributed randomly but homogeneously in the IR^3 material space (three-dimensional Euclidean space). The basic quantitative characteristic of Y^3 are: the pore density, N_V, and the distribution function as the density of pores with their size less than a given value. The measurement of N_V parameter and $N_V(D)$ function by stereological methods is an indirect procedure, which based on direct measurements of quantitative characteristics of set with a known geometrical object [30].

Microscopy based techniques for pore size characterisations provide a powerful tool for characterisation of pore size, size distribution and morphology. They involve direct observation of pores and the consequent determination of size based on a defined measure of diameter. Equivalent circle diameters are used when size determination is conducted by evaluating the projected profile of a pore.

4. Results

4.1. Porosity

The results for the measurements performed in this study are illustrated in Figs. 3 and 4 and summarised in Table 2. Figure 4 illustrates an example of a sample (after mounting, grinding and polishing) along with a digitised image showing the area measurement (Fig. 3).

As shown in Table 2, the measured values of mean equivalent circular diameter (ECD) and pore mean area from specimens sintered at 1250°C were consistently lower, than those from the other measurements for 1120°C for all cooling rates.

Results of this analysis are displayed in Figs. 5–8, which are plots of the fraction of the data subset as a function of porosity parameters. These plots show the fraction of the total pores that demonstrated a given porosity parameter. The solid rhombic lines indicate the distributions for samples cooled at cooling rate 4.5°C/min, while the dashed quadratic and triangular lines show the distribution for samples cooled at cooling rate 31°C/min and 65°C/min, respectively.

However, the plot also shows there is a significant difference in the perimeter levels seen between the two sintering temperatures, with the cooling rate combination showing significantly reduced levels. No significant difference is seen in the slowly and rapid cooled samples. The pores were rounded in specimens sintered at 1250°C.

TABLE 2

Porosity measurement of Fe-3%Mn-0.8%C PM steels

Sintering temperature 1120°C					
Cooling rate, °C/min		Pore area, μm²	Pore perimeter, μm 1120 i 1250°	ECD, μm	Pores area fraction
4.5	mean value	13.77	12.59	2.97	0.083
	median	3.25	6.76	2.04	–
31	mean value	16.02	14.21	3.21	0.105
	median	3.98	7.61	2.25	–
65	mean value	17.66	14.83	3.36	0.127
	median	3.98	7.71	2.25	–
Sintering temperature 1250°C					
Cooling rate, ° C/min		Pore area, μm2	Pore perimeter, μm	ECD, μm	Pores area fraction
4.5	mean value	11.33	11.09	2.59	0.086
	median	2.17	5.56	1.66	–
31	mean value	11.94	10.70	2.47	0.114
	median	1.45	4.60	1.36	–
65	mean value	6.34	8.82	1.80	0.176
	median	0.90	3.86	1.07	–

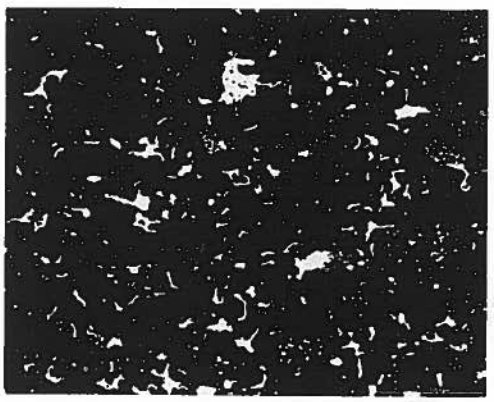

Fig. 3. The negative of digital image of polished cross section of Fe-3%Mn-0.8%C specimen showing typical pores

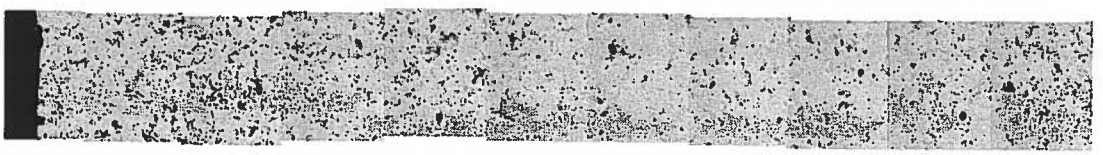

Fig. 4. Section micrographs of polished test specimen showing an example of the whole cross section area obtained vertically along the height of the 55×10×5mm (height × width × length) rectangular specimen

Significantly more internal porosity was observed in the samples sintered at 1250°C. As was shown in Table 2, all measured porosity fraction values for these samples were higher in the contrary to the samples sintered at 1120°C. A reasonable explanation for this could be that Mn is trapped in the closed pores and, after sublimation, the vapours are unable to migrate to the surface due to the lack of opened pores. These trapped vapours are then preserved as Mn oxides in the compact after cooling. Due to this observed increase in porosity in samples rapid cooled after sintering, efforts were made to mitigate the porosity through a procedural change. The data supports the hypothesis that this technique should help minimise porosity, since the Mn is vaporised before the pore is closed. Significantly lower porosity was observed in samples made using furnace-cooling technique.

4.2. Mechanical properties

During investigations, the green and as-sintered densities, microhardness and microstructure, yield ($R_{0.2}$ offset) and ultimate strengths in tension (UTS) tensile elongation (A) and bending (TRS) were determined for at least 20 specimens (Tables 3-5). Density of samples varied from 6.87 gcm^{-3} to 7.02 gcm^{-3} and from 6.91 gcm^{-3} to 7.03 gcm^{-3}, for green and as-sintered samples, respectively. Cross-sectional hardness was changed with increasing cooling rate from 217 HV30 up to 318 HV30 and from 239 HV30 up to 335 HV30, for steels sintered at 1120°C and 1250°C, respectively.

The higher sintering temperature resulted in more rounded porosity and slight improvement in mechanical properties (cf. Table 5). Slow cooling rates favoured plasticity. Cooling below 4.5°C/min produced pearlite with attendant ductility (1.0-1.7%) and strengths up to 595 MPa (tensile) and 1330 MPa (TRS). At higher cooling rates less homogeneous, macroscopically brittle microstructures comprising pearlite, bainite, martensite and retained austenite resulted.

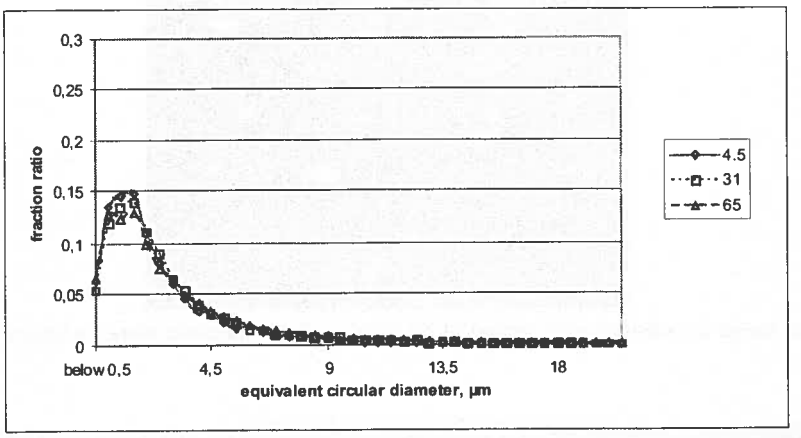

Fig. 5. Graphical representation of the equivalent circular diameter distribution for specimens sintered at 1120°C and cooled with 4.5, 31, and 65°C/min cooling rates

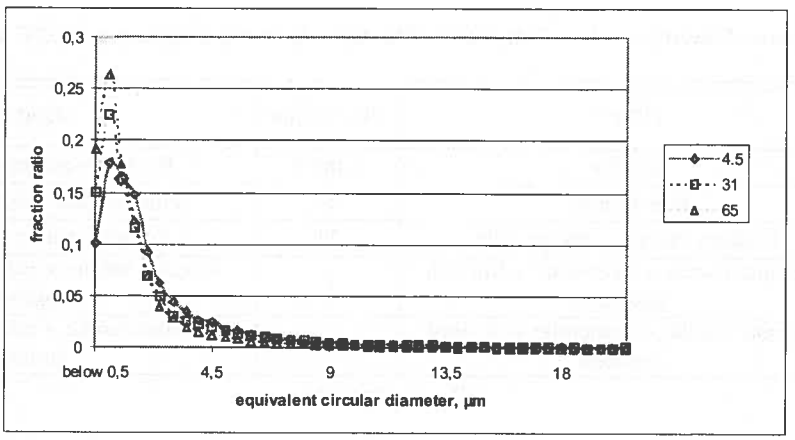

Fig. 6. Graphical representation of the equivalent circular diameter distribution for specimens sintered at 1250°C and cooled with 4.5, 31, and 65°C/min cooling rates

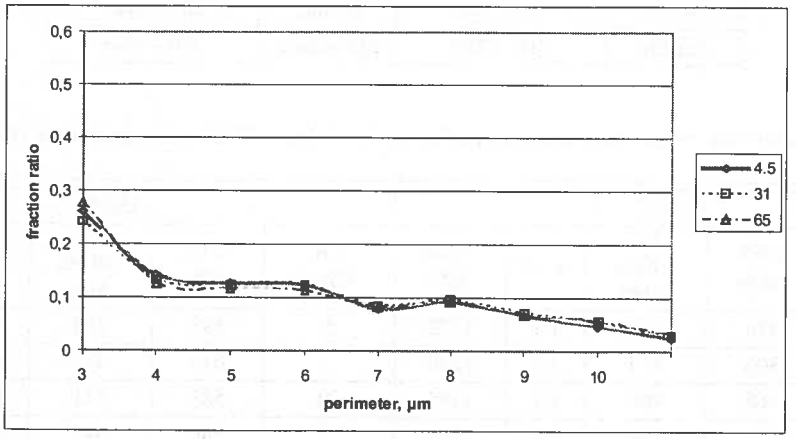

Fig. 7. Graphical representation of the pore perimeter distribution for specimens sintered at 1120°C and cooled with 4.5, 31, and 65°C/min cooling rates

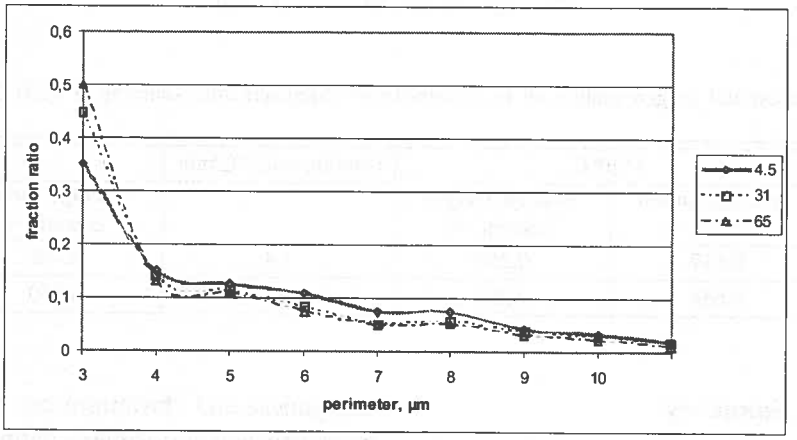

Fig. 8. Graphical representation of the pore perimeter distribution for specimens sintered at 1250°C and cooled with 4.5, 31, and 65°C/min cooling rates

4.3. Chemical analyses

Chemical analyses of these sintered Mn steels (Table 6) showed, in addition to minor Mn losses, some (0.2-0.3 %) decarburization of the steels with concurrent oxygen losses of up to 0.1%. So, although the steels nominally contained 0.8 %C, the actual carbon contents of specimens sintered at 1120°C and 1250°C were ~0.6%C and ~0.5 %C, respectively.

TABLE 3

Microstructure of investigated Fe-3%Mn-0.8%C PM steels. Sintering temperature 1120°C and 1250°C

CR, °C/min	1120°C	CR, °C/min	1250°C
5 and 9	Pearlite	5 and 9	Pearlite + proeutectoid ferrite
16	Fine pearlite	20	Fine pearlite + feathery bainite
30	Feathery bainite + fine pearlite	32	Acicular bainite + martensite
47	Acicular bainite + martensite + Mn-rich austenite	41	Acicular bainite + martensite + retained austenite
above 55	Acicular bainite + martensite + retained austenite	above 57	Acicular bainite + martensite + retained austenite

CR – cooling rate

TABLE 4

Microstructure HV 0.05, of the constituents existed in Fe-3%Mn-0.8%C sintered steels.

Constituent	Hardness HV 0.05	Constituent	Hardness HV 0.05
Ferrite	95 – 160	Bainite	280 – 440
Pearlite	210 – 260	Martensite	580 – 690

TABLE 5

The effect of cooling rate on the mechanical properties of Fe-3%Mn-0.8%C steels sintered at 1120°C and 1250°C

1120°C					1250°C				
CR, °C/min	UTS, MPa	$R_{0.2}$ offset, MPa	A, %	TRS, MPa	CR, °C/min	UTS, MPa	$R_{0.2}$ offset, MPa	A, %	TRS, MPa
5	478	380	1.1	1272	5	595	460	1.6	1327
9	506	414	1.0	1230	9	614	477	1.2	1310
16	568	460	1.1	1195	20	583	511	1.6	1210
30	557	516	0.6	1124	32	586	545	0.6	1193
47	559	478	0.7	1100	41	521	442	0.6	1080
55	535	518	0.6	954	57	491	404	0.6	1097
64	486	ND	0.6	1060	62	507	ND	0.6	993

CR – cooling rate, ND – not defined

TABLE 6

Results of carbon and oxygen analysis of Fe-3%Mn-0.8%C compacts after sintering at 1120°C and 1250°C

Cooling rate, °C/min	1120°C		Cooling rate, °C/min	1250°C	
	Average carbon content, %	Average oxygen content, %		Average carbon content, %	Average oxygen content, %
1.3	0.617	0.250	1.4	0.496	0.130
65	0.658	0.201	65	0.530	0.151

5. Summary

The majority of sinter-hardened steels developed or investigated usually contain copper and nickel in addition to molybdenum and sometimes chromium and manganese [22, 23, 37]. Since elemental nickel is classed as carcinogenic [38] and copper prevents steel recycling, it was than worth of investigation Mn-rich compositions. The processing drawbacks associated with oxidation of manganese and chromium can be solved by sintering in hydrogen rich atmospheres with low dew point [1, 2, 11] and/or use of semi-closed containers and getters to attain the required dry microclimate. Additionally these problems are reduced at higher sintering temperatures, which further promote homogeneity and pore rounding. All data gathered in the present work indicates, that Cu [and

Ni]-free manganese steels are capable of sinter hardening, even in conventional PM processing furnaces.

Only minor dimensional changes resulted from sintering; the average densities were near 7.0 g/cm^{-3}. The main microstructural features and their microhardness are summarised in Tables 3 and 4. The microstructures of the specimens sintered at the lower temperature had finer grain sizes, but also reflected the compositional inhomogeneity in the contrary to the specimens sintered at 1250°C. Therefore the characteristic features described in Table 1 are not a complete microstructural description.

In manganese steel the porosity can be either primary or secondary or a combination of the two, referred to as dual porosity. Primary porosity is the inter-granular porosity inherent to the iron powder, generated at the time of compacting. Secondary porosity is the porosity created by post-forming processes, e.g. sublimation, melting, evaporation or dissolution of the manganese and/or ferromanganese particles. Investigated Mn steels are characterized by their dual porosity: they contain both primary (micropore) and secondary (mesopore) porosity systems. The primary porosity system contains the vast majority of the gas-in-place, while the secondary porosity system provides the conduit for manganese vapour mass transfer to the iron powder and sintering microatmosphere. Primary porosity water vapour and oxygen storage is probably dominated by adsorption. The primary porosity is relatively impermeable due to small pore size. Mass transfer for each gas molecular species is dominated by diffusion that is driven by the concentration gradient. Manganese vapour flow probably mainly through the secondary porosity. When the natural porosity system pressure drops below the critical desorption pressure at given temperature, water vapour and oxygen starts to desorb from the primary iron particles interface and is released into the porosity system. As a result, the adsorbed and combined oxygen concentration in the primary porosity system is reduced. This reduction creates a concentration gradient that results in mass transfer by diffusion through the micro and mesoporosity. Combined oxygen continues to be released as the temperature is increased, and oxides are accumulated in secondary mesopores (Fig. 9) [11].

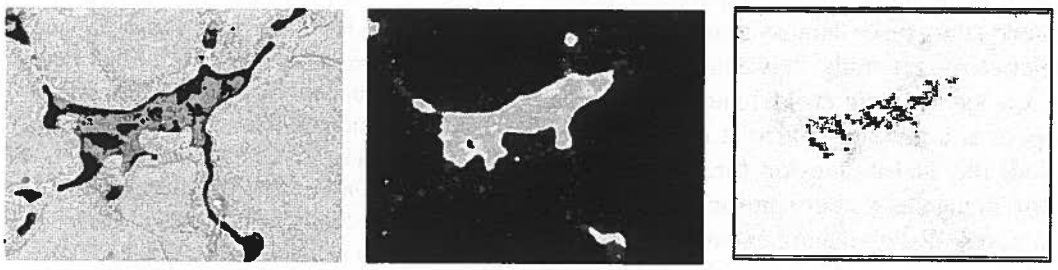

a) SEM image b) Mn X-ray dot map c) O X-ray dot map

Fig. 9. Typical oxide networks of Fe-3%Mn-0.8%C (sponge iron powder + ferromanganese powder) alloy sintered at 1120°C in a poor dew point of about -15°C [11]

Further experimental observations have allowed us to refine and confirm some aspects of our recently proposed mechanism for diffusion between ferromanganese particle and iron powder compact, particularly regarding the prediction of Mn vapour as the dominant diffusing species and the nature of the dependence of ferromanganese particle morphology on the presence of voids in the Fe. Šalak obtained his most promising results using an iron powder produced using an eddy mill technique to disintegrate iron wire mechanically (Hametag powder) [26].

Overall, presented results show there is a greater tendency for porosity to occur in samples made in higher sintering temperature conditions (1250°C) than those made in lower temperature sintering (1120°C), regardless of which cooling rate is used. The hypothesised reason for this is that manganese vaporised (sublimed) and was trapped in the pores. With the presence of oxygen and water vapour, even in the reduced dew point cases, it reacts with this vapour and/or resublimed into the pores seen in these measurements. The secondary porosity is originated from the sublimation of ferromanganese particles.

One of the biggest effects of any change in capillary pore space properties is on the diffusivity of the manganese vapour. Clearly, if one size system is still penetrated when a smaller size is not, at the same overall porosity, then there could be a significant difference between the diffusivities of the two, even though the larger system will be connected through smaller pores. It is

clear that as the capillary porosity penetration threshold decreases, the diffusivity at a given porosity increases because the pore space is better connected farther away from its percolation point. As the capillary porosity decreases, the effect of the capillary porosity also decreases, with the overall permeability being controlled by the amount and diffusivity of the Mn vapour phase. Since at any given capillary porosity, the opened pore fractions of all the different size systems are not the same, the diffusivities should become not similar once the porosity has passed the vapour penetration threshold for sintered compact system.

To utilise to the maximum extent the effect of sublimation and condensation of manganese vapours on alloying, iron compacts must have mainly opened pores, at least at the start of sintering, ensure that by filling these pores the manganese vapours can affect the surface of all particles [21]. Closed pores can develop in PM steels in a wide variety of ways connected with their fabrication route, heat treatment or deformation. Examples of these types in Mn steels are primary pores and sintering secondary pores when manganese particles sublime leaving large pores behind. The sublimation of manganese and disappearance of the ferromanganese particles at sintering temperature takes place almost immediately [27, 28]. The distinction is generally between pores which contain a very low gas pressure (voids) and pores which contain Mn vapour at a pressure which at least balances (and may exceed) the surface tension forces (*bubbles*). In physics of the manganese steel sintering we shall in general refer to pores, distinguishing between voids and bubbles only where necessary. However, this distinction is rarely meaningful since it is generally very difficult to determine the gas pressure inside a cavity. The empirical dividing line between "voids" and "bubbles" is then simply that on sintering voids generally shrink while bubbles remain the same size or grow.

Resolution of the porosity effects on permeability and diffusivity is very difficult. Permeability is fundamentally an intermediate-scale spatially-averaged property that depends on a range of microscopic properties, including the network properties of pores, which often form a significant secondary porosity and permeability in sintered materials.

Water vapour and oxygen alone do not significantly contribute to porosity. However, they form oxides whose morphology affects sintering. Mn and O form oxide, which is network like. In the absence of reducing microatmosphere, the length of the oxide network like phase increases with increasing the oxygen content of the alloy and with decreasing cooling rate. On the other hand, in the presence of reducing microatmosphere, the effect is reversed. Oxide network heavily blocks the manganese interparticle diffusion and hinders homogenisation. This morphology impedes densification and leads to porosity. Finally, sintering temperature and atmosphere play the most significant role in sintering process.

It has been shown that total porosity appears to be the first-order factor in determining the strength of the Mn steels; however, the distribution of porosity likely has a secondary effect on strength. The trends in the ultimate strength versus (total) porosity data indicate that, although there is a large scatter in the data, there is a correlation between strength and porosity.

Acknowledgements

The financial support of the Ministry of Science and Higher Education under the AGH contract no 11.11.110.788 is gratefully acknowledged.

REFERENCES

[1] A. S. Wronski, A. Cias, P. Barczy, M. Stoytchev et al, "Tough Fatigue and Wear Resistant Sintered Gear Wheels", Final Report on EU Copernicus Contract No. ERB CIPA CT-94-0108, European Commission, 1998.

[2] A. Cias, S. C. Mitchell, A. S, Wronski, Proc. 1998 Powder Metallurgy World Congress, EPMA, Granada, Spain **3**, 179-184, (1988).

[3] A. Cias, S. C. Mitchell, A. Watts, A. S. Wronski, Powder Metallurgy **42**, 3, 227 (1999).

[4] S. C. Mitchell, A. S. Wronski, A. Cias, M. Stoytchev, Proc. PM^{2}TEC'99, MPIF, Princeton, New Jersey **7**, 129-144, (1999).

[5] M. Sulowski, A. Cias, Inzynieria Materialowa **2**, 4, 1179 (1998).

[6] P. K. Jones, K. Buckley-Golder, H. David, R. Lawcock, D. Sarafinchan, R. Shivanath, L. Yao, Proc. 1998 Powder Metallurgy World Congress, EPMA, Granada, Spain **3**, 155-166, (1988).

[7] C. Lindberg, Proc. PM^{2}TEC'99, MPIF, Princeton, New Jersey **7**, 229-244, (1999).

[8] P. K. Jones, K. B. Goder, R. Lawcock, R. Shivanath, Proc. PM World Congress on PM and Particulate Materials, MPIF, Princeton, New Jersey 4, p. **13**, 439-450, (1996).

[9] R. Shivanath, P. K. Jones, R. Lawcock, Proc. PM World Congress on PM and Particulate Materials, MPIF, Princeton, New Jersey 4, p. **13**, 427-437, (1996).

[10] M. Youseffi, S. C. Mitchell, A. S. Wronski, A. Cias, Powder Metallurgy **43**, 4, 353 (2000).

[11] S. C. Mitchell, The Development of Powder Metallurgy Manganese Containing Low-Alloy Steels, Ph.D. thesis, (2000), University of Bradford.

[12] A. Cias, M. Stoytchev, A. S. Wronski, Proc. PM²TEC 2001, MPIF, Princeton, New Jersey **10**, 131-140 (2001).
[13] A. S. Wronski, B. S. Becker, C. S. Wright, S. C. Mitchell, Proc. DFPM'99, edited by L. Parilak and H. Danninger **1**, 155-166, (1999).
[14] S. C. Mitchell, B. S. Becker, A. S. Wronski, Proc. 2000 Powder Metallurgy World Congress, Kyoto, K. Kosuge and H. Nagai, Eds., (2001), The Japan Society of Powder and Powder Metallurgy, Part **II**, 923-926, (200).
[15] A. Šalak, M. Selecka, R. Bures, TU Wien Workshop "Sintering Atmospheres for Ferrous Components" Höganäs Chair, 10-11.09.1999.
[16] A. Cias, S. C. Mitchell, K. Pilch, H. Cias, M. Sulowski, A. S. Wronski, Powder Metallurgy **46**, 2, 165 (2003).
[17] A. Cias, M. Sulowski, S. C. Mitchell, A. S. Wronski, Proc. of PM2001, organized by EPMA, Nice **4**, 246-251, (2001).
[18] A. Šalak, Proc. DFPM'96, Ed. by L. Parilak, H. Danninger, J. Dusza, B. Weiss, IMR-SAS Kosice **1**, 205-210, (1996).
[19] M. Sulowski, Ph. D. Thesis, AGH-UST, Cracow, 2003, in Polish.
[20] A. Cias, Development and Properties of Fe-Mn-(Mo)-(Cr)-C Sintered Structural Steels, (AGH-UST, Uczelniane Wydawnictwo Naukowo-Dydaktyczne, Cracow 2004).
[21] A. Šalak, V. Miskovič, E. Dudrova, E. Rudanova, Powder Metallurgy International **6**, 3, 128 (1974).
[22] A. S. Wronski, A. Cias, Proc. PM 2004 World Congress & Exhibition **3**, 1-6, (2004).
[23] A. S. Wronski, A. Cias, Powder Metallurgy Progress **3**, 3, 119 (2003).
[24] S. C. Mitchell, A. Cias, Powder Metallurgy Progress **4**, 3, 132 (2004).
[25] A. Šalak, International Journal of Powder Metallurgy and Powder Technology **16**, 4, 369 (1980).
[26] A. Šalak, Powder Metallurgy International **12**, 2, 72 (1980).
[27] A. Šalak, Powder Metallurgy International **18**, 4, 266 (1986).
[28] A. Šalak, M. Selecká, R. Bureš, Powder Metallurgy Progress **1**, 1, 41 (2001).
[29] ASTM Committee E-4, Standard Practice for Determining the Inclusion or Second-Phase Constituent Content of Metals by Automatic Image Analysis. Annual Book of ASTM Standards 2001, Sect. 3, **03.01**, 2001.
[30] G. Matheron, Journal of Microscopy, no 95, 15 (1972).
[31] T. Allen, Particle size analysis: Classification and sedimentation methods, 1st Eng. Lang. Ed., Chapman and Hall, London, 1994.
[32] L. Svarovsky, Characterization of powders, in Principles of powder technology, N.J. Rhodes, ed., John Wiley & Sons, Chicester, 35, 1990.
[33] R. Davies, Particle size measurements: Experimental techniques in handbook Powder science and technology, M.E. Fayed and L. Otten, eds., Van Nostrand Reinhold Company, New York, 31, 1984.
[34] Ya. E. Gieguzin, Physics of Sintering, Ed. Science, Moscow 1984.
[35] H. Masuda, K. Iinoya, Journal of Chemical Engineering Japan **4**, 1, 60 (1971).
[36] ISO/CD 13322 Particle Size Analysis-Image Analysis Methods, International Organisation for Standarization, Geneva.
[37] F.Chagnon, D. Barrow, Powder Metallurgy **41**, 115 (1998).
[38] EU Carcinogen Directives 90/394/EEC and 91/322/EEC.

Received: 30 May 2008.